Characterization of THB1, a *Chlamydomonas reinhardtii* truncated hemoglobin: Linkage to nitrogen metabolism and identification of lysine as the distal heme ligand

Eric A. Johnson, Selena L. Rice, Matthew R. Preimesberger, Dillon B. Nye, Lukas Gilevicius, Belinda B. Wenke, Jason M. Brown, George B. Witman*, and Juliette T. J. Lecomte*

Supporting Information

Table S1: qPCR probes (ZEN™ Double-Quenched, IDT) used for the detection of THB1 cDNA, the reference CBLP cDNA, and BBS4 cDNA. The 5' end of each probe is labeled with 6-FAM™ and the 3' end with Iowa Black®FQ.

		Sequence (5'-3')
THB1		
	Forward	CGCCTTTATGACTTACGTGTTC
	Probe	/56-FAM/TGATCCGCG/ZEN/AGCAGGGCAT/3IABkFQ/
	Reverse	CTCTTGCAGGGTGGAGTC
CBLP		
	Forward	CGAGTGCAAGTACACCATTG
	Probe	/56-FAM/CTGGGACAA/ZEN/GATGGTCAAGGTCTGG/3IABkFQ/
	Reverse	TCAGCTTGCAGTTGGTCAG
BBS4		
	Forward	GTGATAAACGAAACTACCAACTGC
	Probe	/56-FAM/CGAGACAGG/ZEN/AGTTTGAGGAGTGCTTG/3IABkFQ/
	Reverse	ATGAGCGCCTTGATATAGATGG

Table S2: ^{1}H chemical shifts of the heme group in ferrous Y29F rTHB1[a,b]

Assignment	δ (ppm)
1-CH_3	3.04
2-α-vinyl	8.06
2-β-vinyl *cis, trans*	5.74, 5.79
α-meso	9.29
3-CH_3	3.34
4-α-vinyl	7.69
4-β-vinyl *cis, trans*	5.35, 6.04
β-meso	9.13
5-CH_3	2.61
γ-meso	9.32
8-CH_3	3.44
δ-meso	9.40

[a] This variant was studied instead of wild-type rTHB1 because of favorable spectral properties.
[b] Determined in 90% $^{2}H_2O$/10% $^{1}H_2O$ at pH* 9.2, 298 K.

Table S3: ^{1}H chemical shifts of the axial lysine (K53) in ferrous Y29F rTHB1[a]

Assignment	δ (ppm)
Hζ	−7.85
Hε,ε'	−3.32, −1.72
Hδ,δ'	−2.99, −1.43
Hγ,γ'	−2.36. −1.60
Hβ,β'	0.99, 0.84
Hα	3.40

[a] Determined in 90% $^{2}H_2O$/10% $^{1}H_2O$ at pH* 9.2, 298 K.

Table S4: ^{1}H chemical shifts and dipolar contacts of selected heme pocket residues in cyanomet wild-type rTHB1[a]

Residue	δ(ppm)	Contacts
Phe28 (B9)	H: 9.15; α: 4.60; β: 3.93, 3.62; δ: 7.36; ε: 8.98; ζ: 8.21	Tyr29, Val94
Tyr29 (B10)	H: 8.98; α: 4.82; β: 3.59, 3.45; δ: 8.12; ε: 10.20; η: 27.0	Gln54
Leu38	H: 7.49; α 4.52; β: 1.97, 0.93; γ: 1.35; δ: 0.18, 0.59	3-CH_3, 4-vinyl, Val94
Phe41	H: 7.41; α: 3.78; β: 2.20, 1.91; δ: 6.78; ε: 6.60; ζ: 6.22	4-vinyl, 5-CH_3
Phe42 (CD1)	H: 7.60; α: 4.36; β: 4.03, 2.64; δ: 7.37; ε: 8.06	5-CH_3
Gln50 (E7)	H: 8.62; α: 3.48; β: 2.16, 2.06; ε: 8.74, –0.84	
Gln54 (E11)	H: 8.38; α: 4.00; β: 3.3; ε: 11.18, 5.31	Phe28, Tyr29
Phe57 (E14)	H: 8.55; α: 3.33; β: 2.45, 1.64; δ: 6.10; ε: 6.69; ζ: 6.82	1-CH_3, 8-CH_3, Leu73
Tyr68 (E17)	H: 7.73; α: 4.30; β: 2.02; δ: 6.50; ε: 6.37	7-prop, 8-CH_3, Phe57
Leu73 (F4)	H: 9.30; α: 4.27; β: 2.54, 2.12; γ: 1.30; δ: 0.18, –0.99	1-CH_3, 8-CH_3
His77 (F8)	H: 9.74; α: 7.77; β: 9.12, 8.22; δ1: 14.32	Leu73
Asn87 (G1)	H: 11.22; α: 5.08; β: 3.16, 2.75	His90
His90 (G4)	H: 7.02; α: 3.27; β: 2.38, 1.72; δ2: 6.32; ε1: 7.71	3-CH_3, Phe41
Phe91 (G5)	H: 6.82; α: 2.23; β: 3.27, 1.99; δ: 6.43; ε: 7.03; ζ: 7.51	3-CH_3, 2-vinyl
Val94 (G8)	H: 7.11; α: 2.98; β: 0.36; γ: –0.40, –1.23	3-CH_3, 2-vinyl
Val119 (H11)	H: 8.42; α: 3.60; β: 2.33; γ: 1.16, 0.90	2-vinyl
Ala122 (H14)	H: 8.20; α: 4.58; β: 1.81	2-vinyl
Phe127 (H19)	H: 8.20; α: 4.83; β: 3.51, 2.92; δ: 7.41; ε: 6.66; ζ: 6.41	3-CH_3

[a] Determined in 10% $^{2}H_2O$/90% $^{1}H_2O$, pH 7.5, 25 °C, at 2.1 mM protein, with a 1.5-fold excess of KCN.

Table S5: ^{1}H chemical shifts of the heme group (major isomer) in cyanomet Y29F rTHB1[a]

Assignment	^{1}H
1-CH_3	16.1
2-α-vinyl	17.26
2-β-vinyl *cis, trans*	–5.72, –4.45
3-CH_3	12.92
4-α-vinyl	5.45
4-β-vinyl *cis, trans*	–1.04, –0.05
5-CH_3	17.24
6-α-propionate	14.64, 12.37
6-β-propionate	0.50, –0.10
7-α-propionate	6.23, 3.92
7-β-propionate	–1.08, –1.75
8-CH_3	6.11

[a]δ (ppm), determined at 298 K in 90% $^{1}H_2O$ / 10% $^{2}H_2O$ at pH 7.4, 100 mM phosphate, on a 1.3 mM Y29F rTHB1 sample with a five-fold excess of KCN.

Table S6: ^{1}H chemical shifts and dipolar contacts of selected heme pocket residues in cyanomet Y29F rTHB1[a]

Residue	δ(ppm)	Contacts
Phe28 (B9)	δ: 7.49; ε: 8.89; ζ: 8.09	Phe29, Val94, Gln54
Phe29 (B10)	δ: 8.36; ε: 10.46; ζ: 13.91	
Leu38	β: 0.86; γ: 1.33; δ: 0.16, 0.54	3-CH_3, 4-vinyl, Val94
Gln54	ε: 12.66, 7.00	Phe28
Leu73 (F4)	H: 9.20; α: 4.20; β: 2.40, 2.01; γ: 1.10; δ: –0.09, –1.36	1-CH_3, 8-CH_3
His77 (F8)	H: 9.85; α: 7.98; β: 9.18, 8.79; δ1: 15.14	Leu73
Asn87 (G1)	H: 11.29; α: 5.15; β: 3.19, 2.79	His90
His90 (G4)	δ2: 6.32; ε1: 7.74	3-CH_3, Phe41
Phe91 (G5)	δ: 6.45; ε: 6.93; ζ: 7.40	3-CH_3, 2-vinyl
Val94 (G8)	H: 7.05; α: 2.95; β: 0.35; γ: –0.53, –1.18	3-CH_3, 2-vinyl
Ala122 (H14)	H: 8.08; α: 4.40; β: 1.58	2-vinyl

[a] [a]δ (ppm), determined at 298 K in 90% $^{1}H_2O$ / 10% $^{2}H_2O$ at pH 7.4, 100 mM phosphate, on a 1.3 mM Y29F rTHB1 sample with a five-fold excess of KCN. These residues position the heme in its pocket.

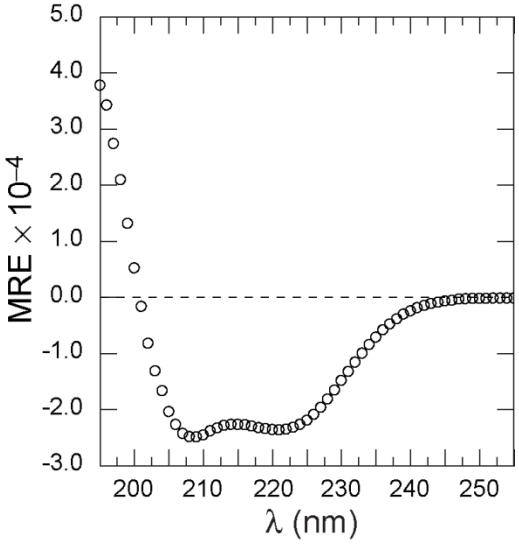

Figure S1: Circular dichroism spectrum (far-UV) of ferric rTHB1 (~20 μM heme, pH 7.3, 25 °C). The molar residual ellipticity (deg cm^2 $dmol^{-1} \times 10^{-4}$) is shown between 195 and 255 nm. The double-minimum shape is characteristic of a high helical content, estimated at ~67% using K2D3.[1] Data were collected on an Aviv 62DS spectropolarimeter (1-nm steps, 5-s averaging time).

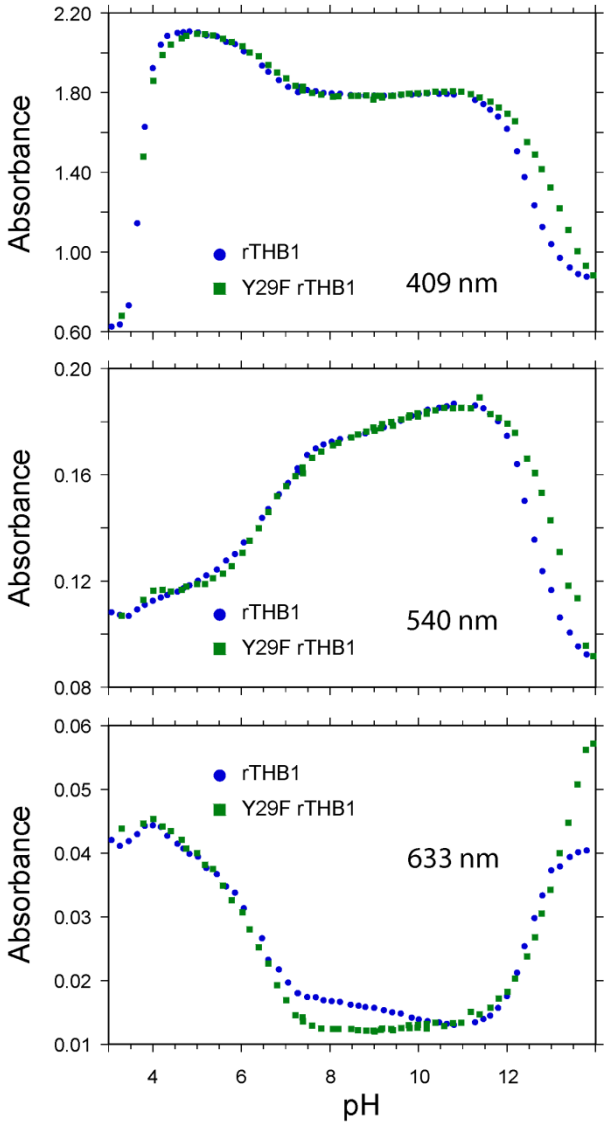

Figure S2: Comparison of the pH titration of ferric wild-type rTHB1 (blue circles) and Y29F rTHB1 (green squares). The response of Y29F rTHB1 differs from that of the wild-type protein at pH values above 11.5 (where the pH measurement becomes less reliable) and in the 7–10 range, where the high-spin marker (633 nm) of the former is completely absent. The overall high similarity of the responses supports that Tyr29 (B10) is not an axial ligand to the iron.

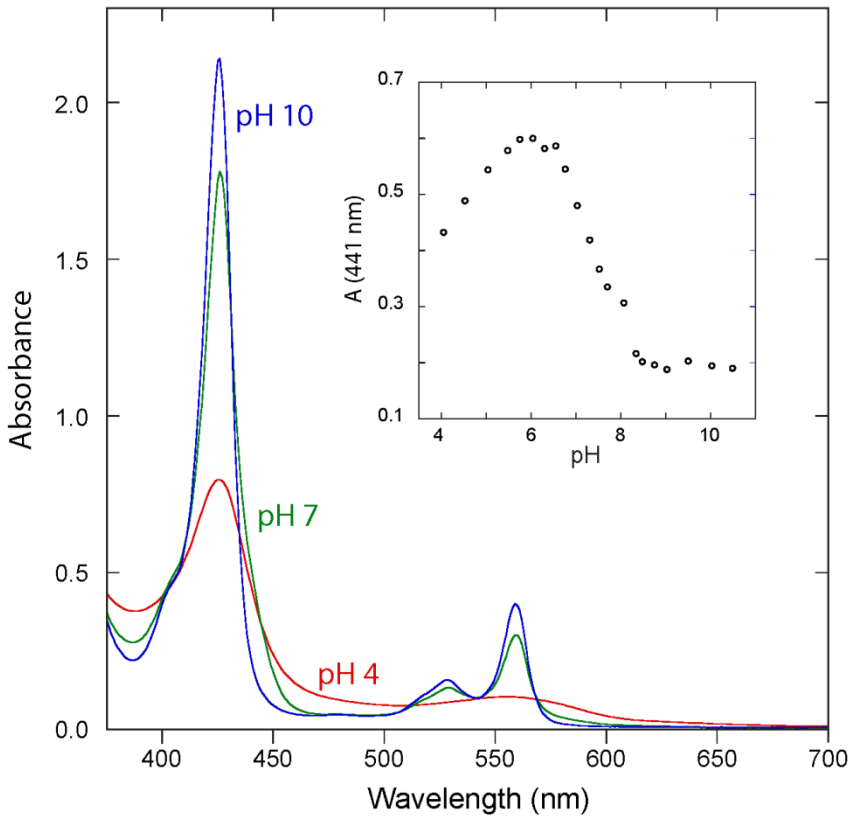

Figure S3: The optical spectrum of ferrous wild-type rTHB1 at three pH values. The intermediate spectrum (green) has a shoulder at ~440 nm and cannot be reproduced with combinations of the other two spectra. This suggests the existence of additional species in solution. The inset shows the absorbance at 441 nm as a function of pH.

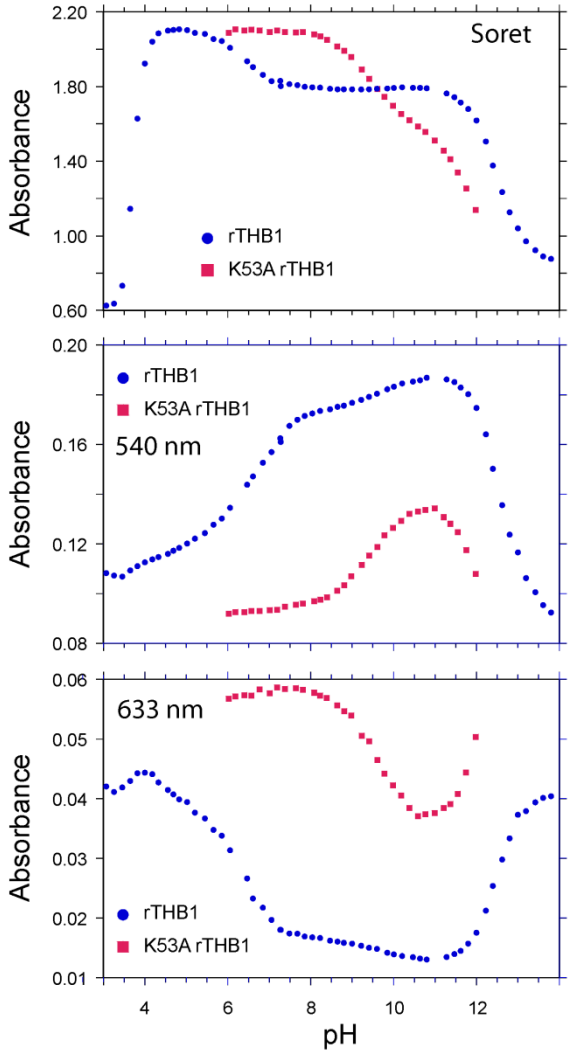

Figure S4: Comparison of the pH titration of ferric wild-type rTHB1 (blue circles) and K53A rTHB1 (red squares). The response of K53A rTHB1 differs from that of the wild-type protein. "Soret" is 409 nm in wild-type and 406 nm in K53A THB1. Data were scaled to the same absorbance of the aquomet state for comparison. The high-spin marker (633 nm) persists to pH 10 in the variant.

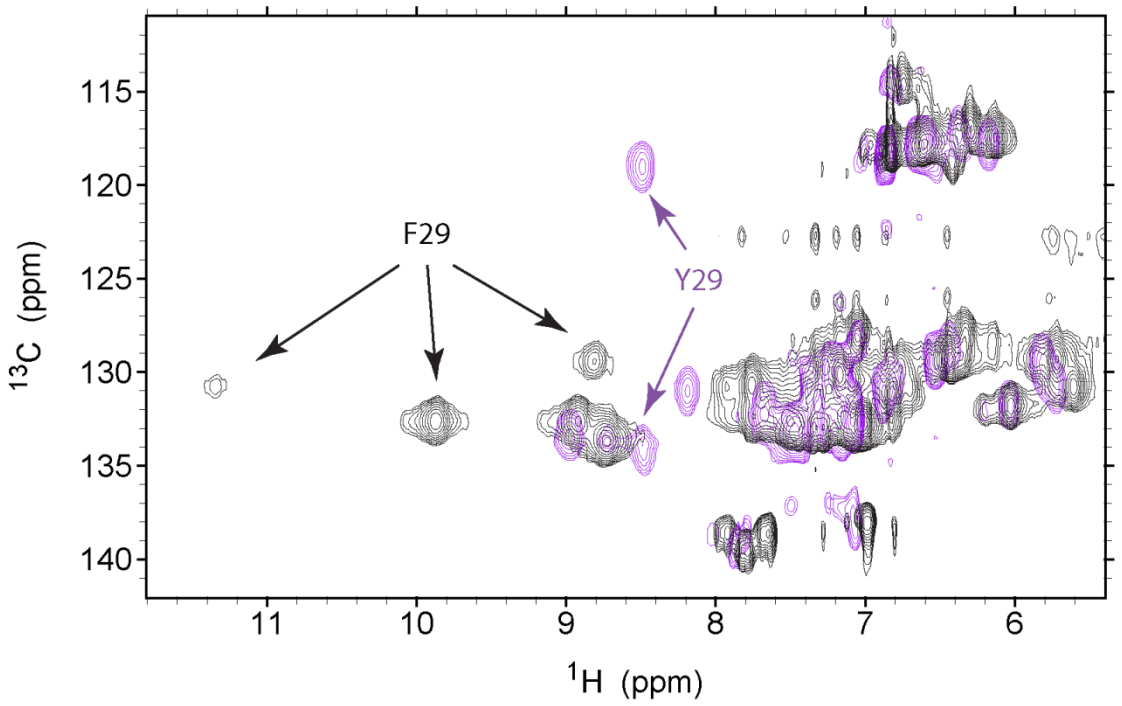

Figure S5: The aromatic region of the natural abundance ^{1}H-^{13}C HMQC spectra collected on wild-type (purple) and Y29F (black) rTHB1 in the ferric state and without added exogenous ligand. The ring signals of Tyr29 and Phe29 are indicated. Data were collected in $^{2}H_2O$, pH* 8.0, 308 K.

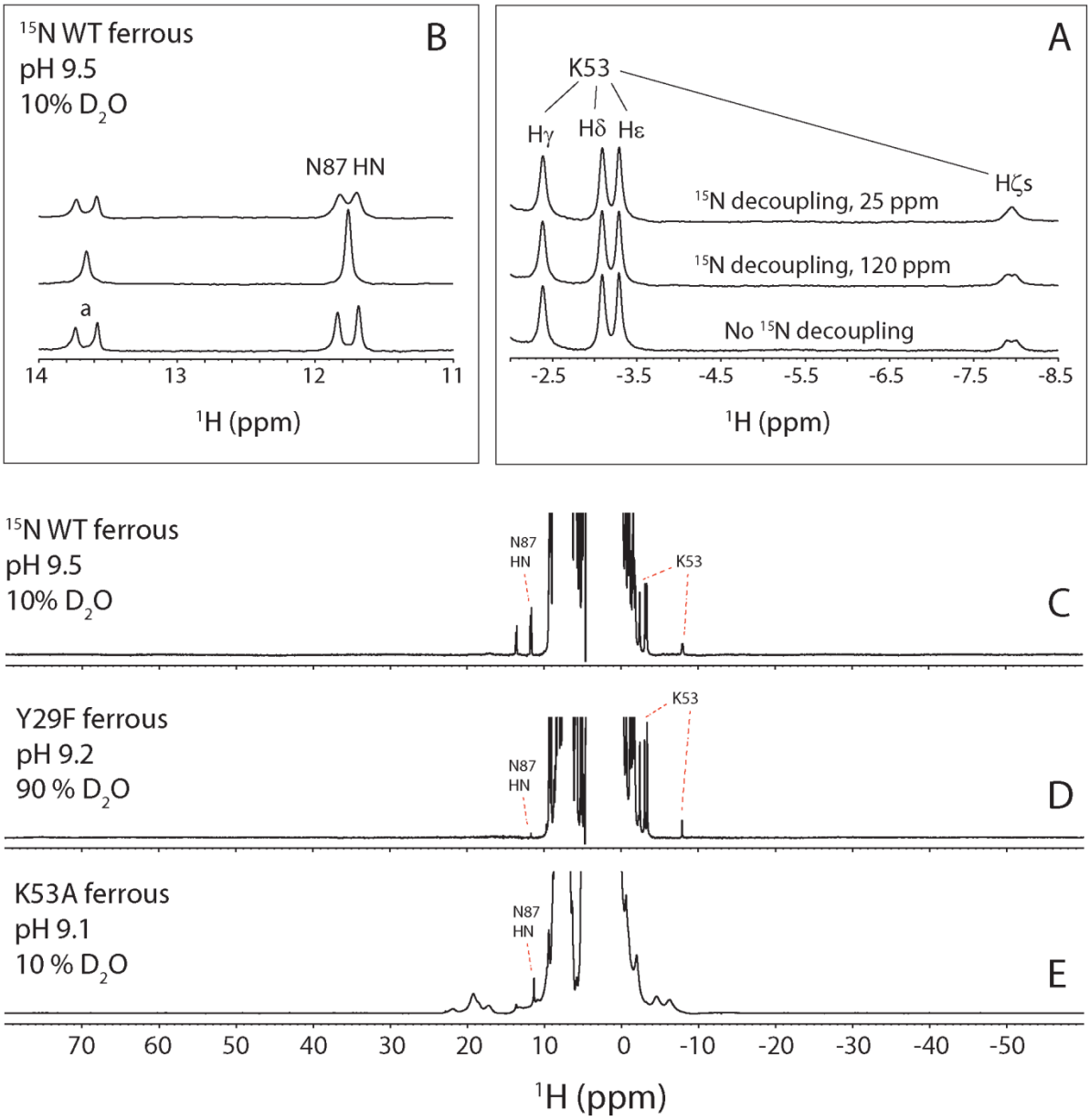

Figure S6: Assignment of K53 NζH$_2$. (A) The highly upfield −8 ppm signal is split into a doublet in ^{15}N labeled ferrous wild-type (WT) rTHB1. Broadband ^{15}N decoupling applied in the Lys Nζ region (~25 ppm) caused the doublet to collapse. (B) In the downfield region, the amide NH of Asn87 and a histidine NεH signal (marked a) are shown for comparison. (C–E) Comparison of the ferrous spectra. The diamagnetic portion of the wild-type and Y29F THB1 spectra is shown in Figure 6 of the main text. The spectrum of ferrous K53A rTHB1 (10% ^{2}H$_2$O/90% ^{1}H$_2$O, pH 9.1) is broad, characteristic of a paramagnetic species and demonstrates the absence of the sixth ligand detected in the wild-type and Y29F proteins.

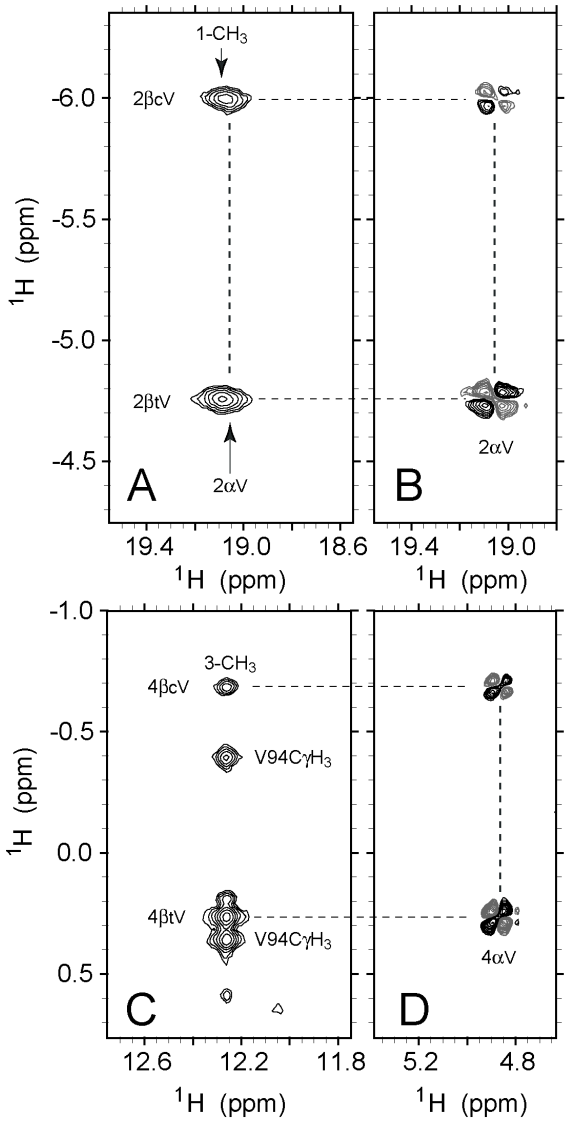

Figure S7: ^{1}H signature of the heme vinyl groups in wild-type cyanomet rTHB1. (A) and (C), NOESY data, (B) and (D), DQF-COSY data. Signals from the 1-CH_3 and adjacent 2-vinyl nearly overlap (panel A). Data were collected in $^{2}H_2O$, pH 7.5 and 298 K.

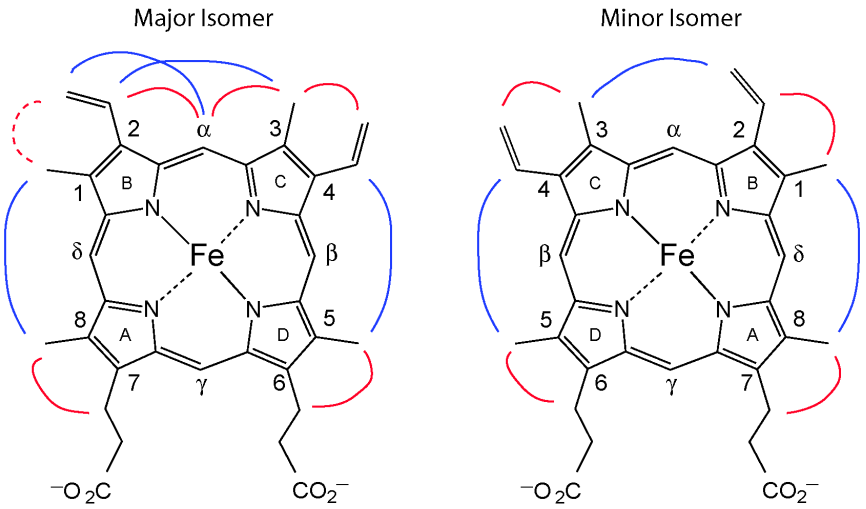

Figure S8: Diagram of intra-heme NOEs observed in the major and minor isomer of wild-type cyanomet rTHB1 (red = strong, blue = weak, dashed = overlapped). The vinyl groups are oriented as indicated by the strength of the dipolar interactions. In both cases, the proximal histidine is between the page and the viewer.

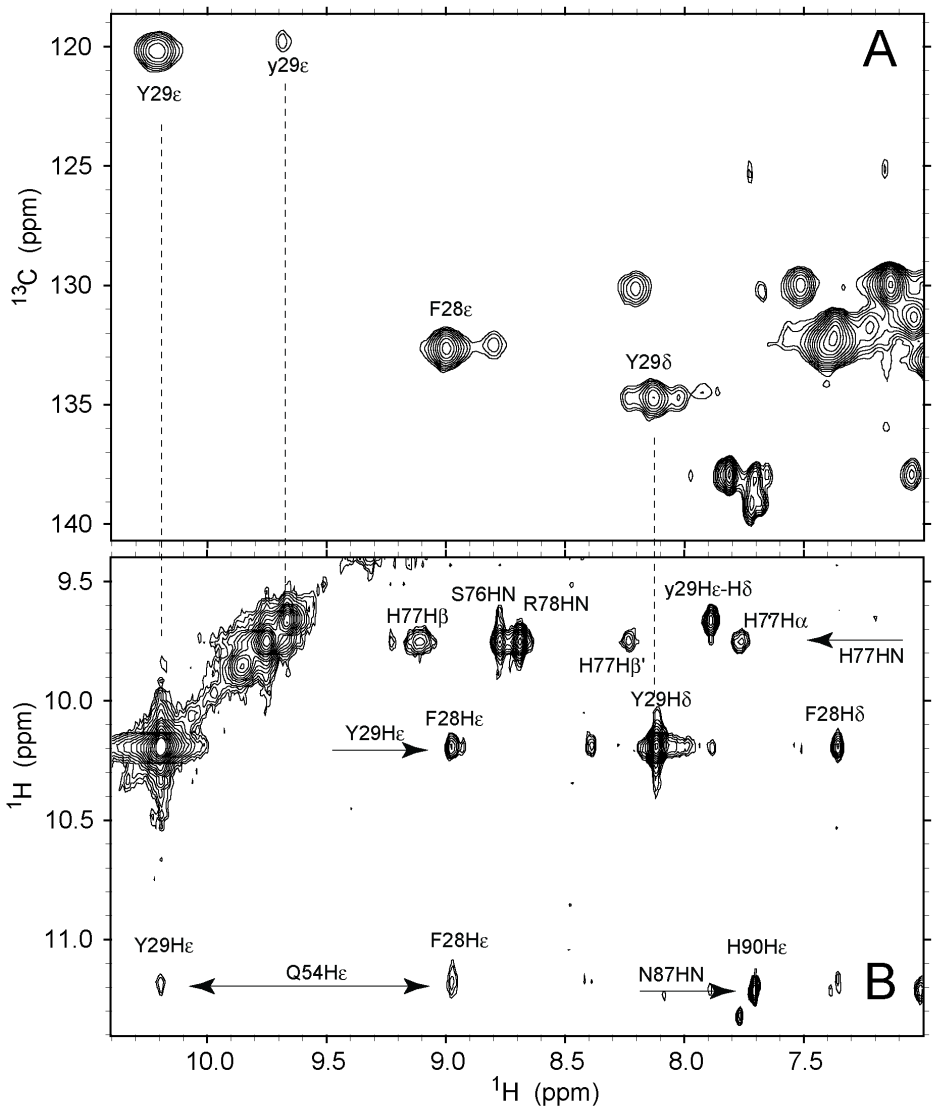

Figure S9: Portions of the natural abundance ^{1}H-^{13}C HMQC (A) and NOESY (B) data showing the ring resonances of Tyr29 (B10) and Phe28 (B9). Data were collected in $^{2}H_2O$, pH 7.5 (A) and 10% $^{2}H_2O$/90% $^{1}H_2O$, pH 8.0 (B). Uppercase residue labels refer to the major isomer; lowercase labels to the minor isomer.

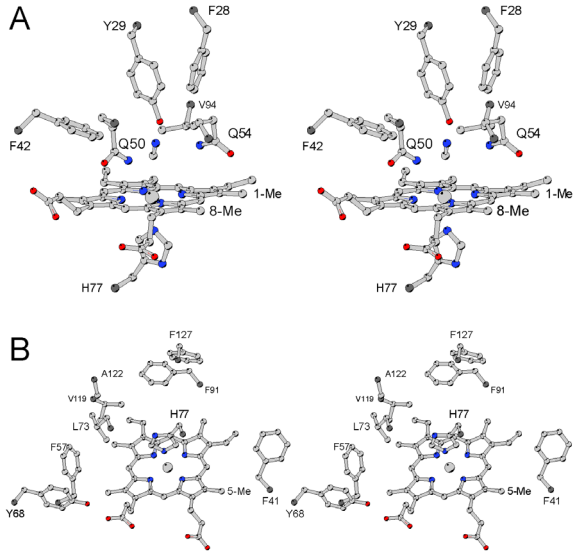

Figure S10: Portions of the cyanomet THB1 structure, modeled after the structure of *C. eugametos* Hb (CtrHb, PDB ID 1DLY) and shown as stereo pairs. (A) The distal side of the heme group. (B) The proximal side of the heme group.

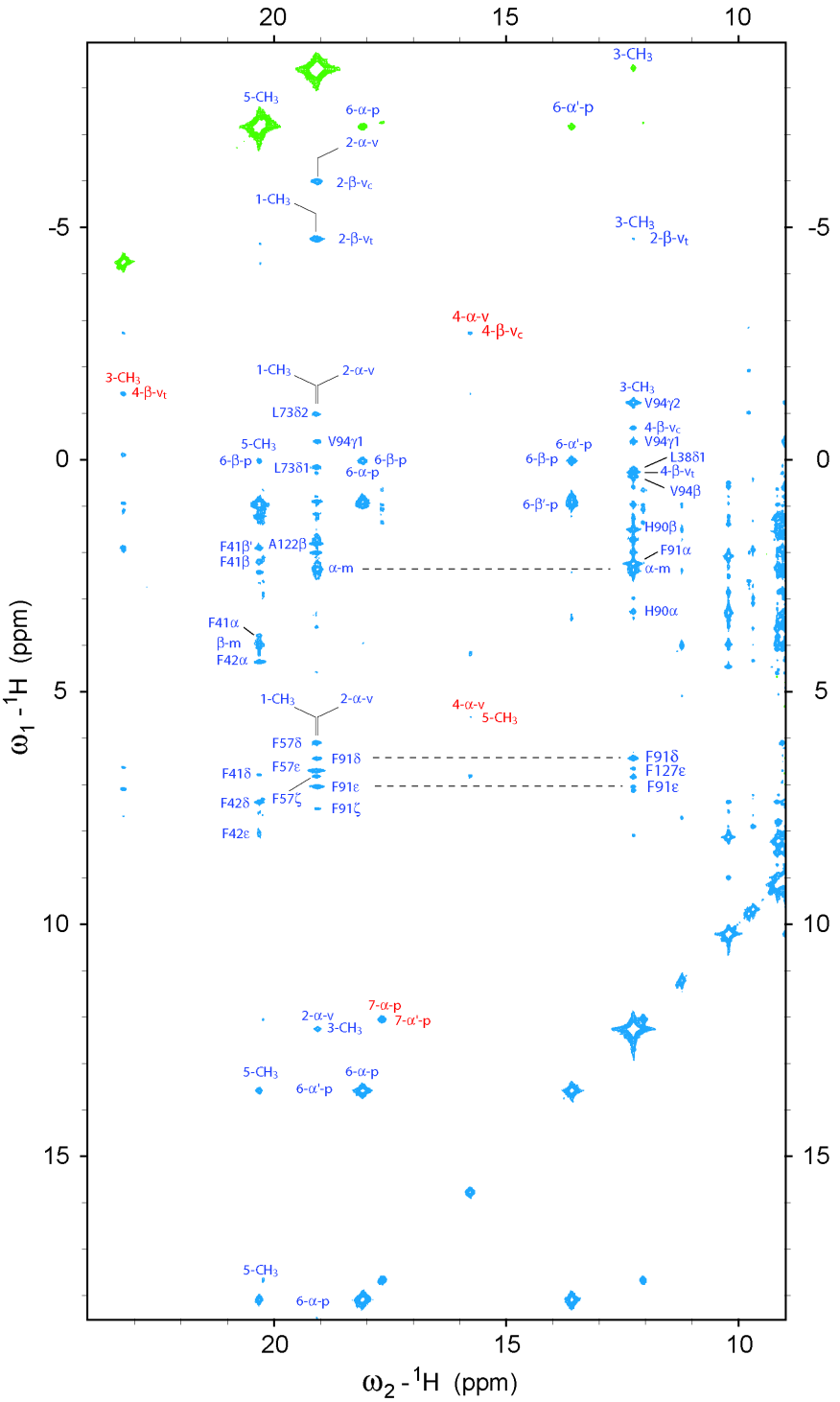

Figure S11: Portion of a NOESY spectrum of cyanomet rTHB1 with a few key NOEs annotated. Blue and red labels correspond to the major and minor heme orientational isomers respectively. Cross peaks in green are folded in the indirect dimension. Data were collected in ^2H_2O, pH 7.5, 298 K.

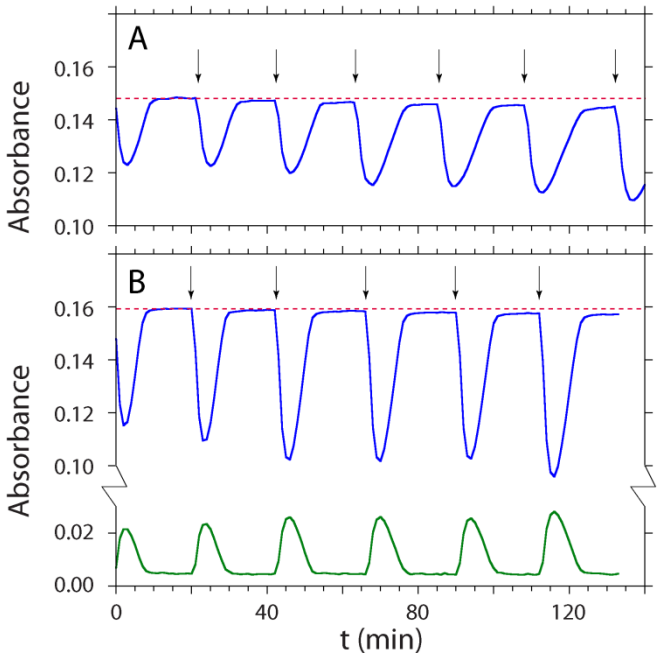

Figure S12: NOD activity of wild-type rTHB1 and Mb. Samples contained ~10 μM protein in 100 mM phosphate buffer, pH 7.1 and a Fd/$NADP^+$ reduction system. (A) Time trace at 545 nm upon repeated addition of 1 eq. MAHMA-NONOate to wild-type rTHB1-O_2. The first addition occurred at t = 0; subsequent additions are marked by the vertical arrows. The data are the same as presented in Figure 11A. (B) Time traces at 543 nm (upper line, blue) and 633 nm (lower line, green) upon addition of 1 eq. MAHMA-NONOate to Mb-O_2. Note the behavior of the charge transfer band, for comparison with K53A rTHB1. The dashed red line indicates the absorbance at the first oxy plateau.

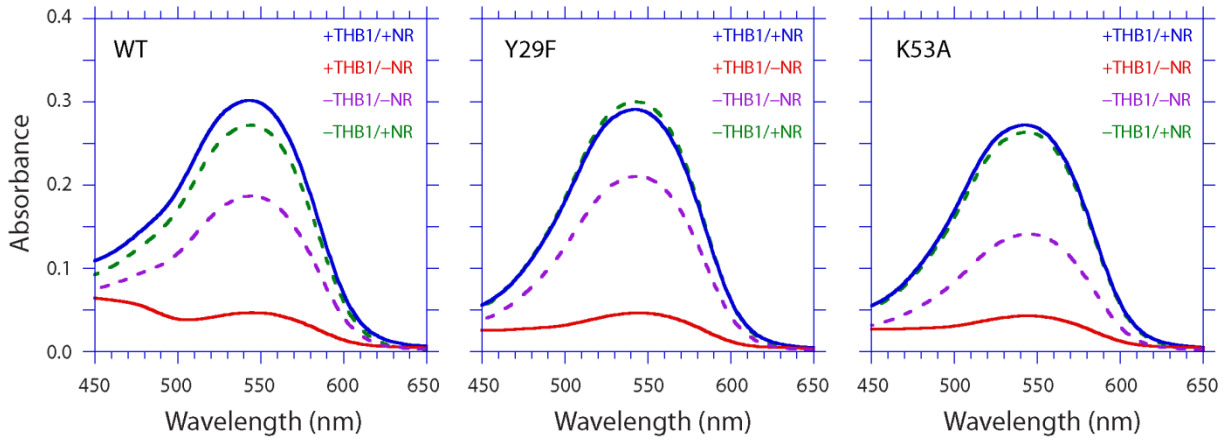

Figure S13: Representative Griess assay results (conditions described in the text) for wild-type, Y29F and K53A rTHB1. In each case, the protein concentration was ~10 μM and 5 additions of MAHMA-NONOate were performed (see Materials and Methods and Figure 11), totaling ~100 μM released $NO^{\bullet}$. –THB1/–NR (dashed, magenta) illustrates nitrite production in the absence of the globin and the nitrate reductase. –THB1/+NR (dashed, green) illustrates nitrate + nitrite production in the absence of the globin; the amount of nitrate produced by background reactions corresponds to the difference between the two dashed curves. +THB1/–NR (red) shows that the globin prevents the production or accumulation of nitrite and demonstrates that under the chosen condition, rTHB1 consumes $NO^{\bullet}$ faster than it disappears through background reactions. +THB1/+NR (blue) demonstrates that the globin catalyzes the production of nitrate. The amount of nitrate produced by the rTHB1 enzymatic reaction corresponds approximately to the difference between the two solid curves. An estimate of the yield (90% and higher) can be obtained using the expected nitrate concentration based on the amount of $NO^{\bullet}$ added (~100 μM). Variants and wild-type rTHB1 show the same qualitative behavior (compare red and blue solid traces in the three panels). The observed differences in nitrate produced when the protein is present are consistent with variations in the total amount of $NO^{\bullet}$ added rather than significant differences in yield.

Note that the –THB1 results depend on the overall experiment time, amount of $NO^{\bullet}$ added, and concentration of the enzyme and substrates used in the assay. The nitrite and nitrate yields in the absence of THB1 demonstrate the existence of competing $NO^{\bullet}$ and RNS reactions, which do not occur on a relevant time scale when rTHB1 is present.

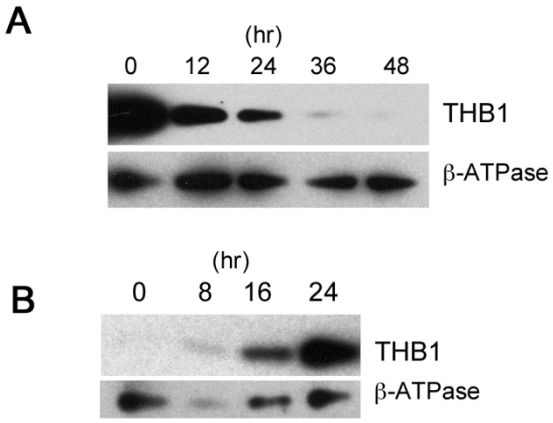

Figure S14: Western blot of the THB1 levels over time as a function of nitrogen source. (A) CC-1690 cells grown until mid-log phase in Sager-Granick M medium, then sedimented by low speed centrifugation and resuspended in Sager-Granick M medium with 7 mM ammonium chloride instead of 3.5 mM ammonium nitrate. Culture started at a cell concentration of 0.5 million cells per mL. At specified time points, whole-cell protein extract prepared from culture sample was stored at −80 °C until use. (B) CC-1690 cells grown until mid-log phase in Sager-Granick M medium with 7 mM ammonium chloride, then sedimented by low speed centrifugation and resuspended in normal Sager-Granick M medium. Samples prepared as in part A. The β subunit of the ATP synthase was used as loading control.

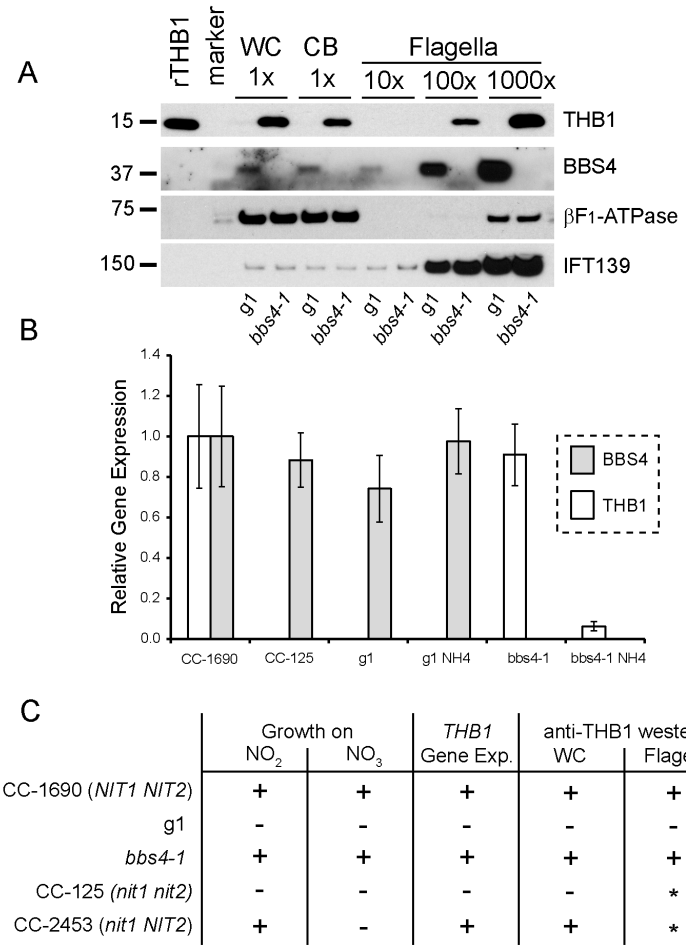

C

	Growth on NO_2	Growth on NO_3	*THB1* Gene Exp.	anti-THB1 western WC	anti-THB1 western Flagella
CC-1690 (*NIT1 NIT2*)	+	+	+	+	+
g1	-	-	-	-	-
bbs4-1	+	+	+	+	+
CC-125 *(nit1 nit2)*	-	-	-	-	*
CC-2453 (*nit1 NIT2*)	+	-	+	+	*

Figure S15: Determination of THB1 expression and Nit1 and Nit2 phenotypes for g1 and *bbs4-1*. (A) Whole cells (WC), cell bodies (CB), and isolated flagella from g1 and *bbs4-1* cells were probed with anti-THB1 and anti-BBS4. Equivalent amounts of cells and cell bodies and 10, 100, or 1000-fold excess flagella were loaded (i.e., 1X is 10^5 whole cells or cell bodies, and 10X flagella is 2×10^6 flagella). Mitochondrial βF_1-ATPase and IFT protein IFT139 served as loading controls. Assuming there is no βF_1-ATPase in flagella, the signal in flagella is a measure of cell body contamination in highly concentrated flagella. Therefore, the level of THB1 in *bbs4-1* flagella is too high to be explained by cell body contamination. Unexpectedly, there is little or no THB1 expression in g1 cells. (B) Transcript abundances of *THB1* and *BBS4* relative to *CBLP*, as determined by qPCR. Averages ± standard deviation of three independent experiments performed on a mixture of biological duplicates are shown. All samples grown in Sager-Granick M medium except "*bbs4-1* NH4" which is strain *bbs4-1* grown in ammonium. (C) Summary of growth on nitrate and nitrite, *THB1* gene expression, and western blotting results. Asterisks indicate flagella that were not tested by western blotting.

Reference

(1) Louis-Jeune, C., Andrade-Navarro, M. A., and Perez-Iratxeta, C. (2012) Prediction of protein secondary structure from circular dichroism using theoretically derived spectra. *Proteins 80*, 374–381.